Research article

Synergistic effect of Mg addition on the enhancement of the mechanical properties and evaluation of corrosion behaviors in 3.5 wt % NaCl of aluminum alloys

Mohammad Salman Haque [*], Modassher Nomani, Azmery Akter, Istiak Ahmed Ovi

Department of Materials Science and Engineering, Khulna University of Engineering & Technology, Khulna-9203, Bangladesh

ABSTRACT

Aluminum alloys are highly preferred for their superior properties, including high corrosion resistance and lightweight in the automotive industry. To better understand how magnesium addition affects aluminum's corrosion and strengthening properties, three different percentages of magnesium-added aluminum alloys, as well as pure aluminum, were melted at a temperature of $800 \pm 10\ ^{\circ}C$ in a furnace and cast using the sand molding process. Subsequently, weight loss was used to conduct corrosion testing along with mechanical tests such as tensile, flexural, hardness, and impact tests. In-depth research revealed that the addition of magnesium at 3 wt %, 5 wt %, and 7 wt % strengthened the aluminum alloy. The addition of magnesium resulted in the formation of Al_3Mg_2, which restricted the movement of dislocation, induced grain refinement, and increased the strength of the alloy. However, it was observed that the addition of magnesium caused a decrease in the alloy's toughness and ductility, resulting in decreased impact energy and % elongation by 29.19 % and 34.87 % respectively by the addition of 5 wt% Mg compared to pure aluminum. Nevertheless, the optical microstructure and SEM image revealed refined grains and the formation of Al_3Mg_2, providing valuable insight into magnesium's strengthening behavior in aluminum. The study found that adding 7 wt % Mg to the aluminum alloy did not significantly improve its strength and hardness compared to adding 5 wt % Mg. This was because the 7 wt % Mg addition caused the grain size to increase, making it less effective at resisting dislocation movements. The grain coarsening of the 7 wt % Mg added alloy was also revealed in the optical microscope and the SEM images. The EDS analysis confirmed the presence of Al and Mg within the globular-shaped intermetallic particles, indicating the formation of the Al_3Mg_2 intermetallic phases. However, the highly reactive nature of magnesium results in a higher corrosion rate in terms of weight loss and corrosion current density, which causes the formation of pits and metal dissolution, leading to significant metal loss beneath the original surface when immersed in 3.5 wt % NaCl medium for a period of fifteen and thirty days. Localized corrosion was indicated by the SEM images, which showed concave and convex structures formed by the corrosion products on the alloys. The breakdown of the Al_2O_3 protective layer, which is the cause of the pits and cracks in the corrosion products, may be brought on by internal stress or the dehydration of hydroxides, which is known as Mg-induced stress corrosion cracking. However, more pits and cracks are found in the SEM image for the 7 wt % Mg addition as it was corroded more compared to the other alloys. The map analysis of the corroded alloy confirmed the corrosion behaviors of

---

* Corresponding author.
E-mail addresses: salmanhaque@mse.kuet.ac.bd (M.S. Haque), mnalif33@gmail.com (M. Nomani), azmery.akter@mse.kuet.ac.bd (A. Akter), ovi1827035@stud.kuet.ac.bd (I.A. Ovi).

the Mg-added alloy by the presence of oxygen all over the surface. Because of the alloy's Al_3Mg_2 intermetallic compound's refinement and lower corrosion rate, 5 wt % of Mg was found to be the optimal amount for the addition of aluminum to increase strength and hardness without compromising the alloy's toughness and ductility.

1. Introduction

Aluminum alloys, known for their high strength-to-weight ratio, formability, and corrosion resistance, have been utilized in various sectors for years due to their beneficial qualities. A matrix of aluminum and a scattered phase of the other elements make up the usual microstructure of aluminum alloys. The properties of the material can be significantly affected by the size, shape, and distribution of these phases. For instance, the strength and hardness of the alloy can be increased by the inclusion of fine, uniformly scattered particles. The final qualities of an aluminum alloy are greatly influenced by how the material is processed, including casting, rolling, forging, and extrusion. Different heat treatments and surface treatments can also be used to improve certain qualities [1,2].

To meet the high-performance demands of the automotive and aerospace industries, aluminum alloys must naturally age to achieve high strength. When these heat treatments are properly combined, maximum strength can be attained. Additionally, solid solution strengthening is used to increase the strength of non-heat-treatable alloys, with pure aluminum, manganese, silicon, and magnesium serving as the alloying components. The 1 xxx, 3 xxx, 4 xxx, and 5 xxx series, respectively, are given to these [3]. Such alloys are subjected to various degrees of cold working or strain hardening to increase their extra strength. By rolling, using dies, or performing other comparable procedures where the area is reduced, plastic deformation is accomplished [4,5].

The superior corrosion resistance and outstanding formability of aluminum-magnesium alloys make them a preferred option for automotive and transportation applications. The thermal characteristics of aluminum alloys are another significant feature. Some aluminum-magnesium alloys that are prone to intergranular corrosion can also be susceptible to stress corrosion. However, this only applies to alloys with a magnesium content of more than 3.5 wt %. Just because a metal is sensitized by precipitation at grain boundaries does not necessarily mean that corrosion will occur, be it intergranular corrosion or stress corrosion cracking. The likelihood of corrosion would also depend on the surrounding environment [6–8]. According to research, silicon and magnesium can be added to aluminum alloys to increase their thermal conductivity and heat resistance. This is especially crucial for high-temperature applications, like those in the aerospace and automotive sectors. Aluminum alloys are a popular option for electrical and electronic applications because of their physical characteristics, which include great electrical conductivity and high reflectivity [9].

The strength of the metal is increased when magnesium is alloyed with aluminum to enhance the strain hardening of the aluminum. Solid solution hardening is the process of merely dissolving magnesium as it integrates into the aluminum's structure to strengthen it. The resultant aluminum alloy undergoes no heat treatment and is transformed into a high-strength material. Extrusion of this metal series might be costly and challenging for a business looking to do so. Rather, the metal is shaped into sheets and plates. Because it can be used for holding tanks, trains, trucks, buildings, and ships, it is appropriate for usage as a structural metal [10]. For this reason, not only higher toughness but also higher strength materials are needed. To develop sustainable materials for innovative uses, the mechanical characteristics and corrosion behavior of the Mg-added aluminum alloy are thus examined in this experiment to determine the ideal concentration of Mg addition for ensuring the best characteristics.

2. Experimental procedure

The preparation of the alloy involved melting commercially pure aluminum as the starting material in a clay-graphite crucible using a gas-fired pit furnace with a flux cover such as a degasser. To introduce alloying elements, commercially pure magnesium was added, and the furnace temperature was maintained at 800 ± 10 °C using an electronic controller during the melting process. The resulting mixture was homogenized under constant stirring at 750 °C [11]. To ensure that the sand mixture used for molding could withstand the high temperature of the Al–Mg alloy, it was carefully prepared consisting of sand, clay, and a binding agent blended to the appropriate consistency and moisture content. The chemical composition of the alloy was analyzed using optical emission spectroscopy (OES) methods, and the presence of trace impurities such as Mn, Si, and Fe was observed (Table 1). Once poured into the mold, the metal was allowed to cool and solidify, contracting to fill the mold cavity and create a solid metal part. The shaping of each end of the workpiece into a rounded, dumbbell shape was accomplished using a cutting tool along with forming tools such as the round nose and cove tools shown in Fig. 1(a). Tensile testing was performed according to ASTM E8 specifications, using an Instron testing machine at room temperature with the sustaining strain rate at $10^{-3}/s$, and the failed sample after the tensile test is shown in Fig. 1(b). Three samples for each type were performed, and the closest average value of the results was used to measure the strength. Three-point

Table 1
Chemical composition of the experimental alloys (mass fraction, %).

Sample name	Mg	Si	Mn	Fe	Al
Pure Al	0.002	0.115	0.0018	0.23	Bal
Al + 3 % Mg	3.16	0.137	0.0017	0.2	Bal
Al + 5 % Mg	5.09	0.154	0.0021	0.25	Bal
Al + 7 % Mg	7.26	0.163	0.0018	0.29	Bal

flexural test was performed on the alloys according to the ASTM D790 standard. The hardness of the machined surface was tested using the Brinell hardness testing machine (AKB-3000) with a 1/8-inch ball in B scale following the ASTM E18-22 standard. The Impact Testing Machine (Charpy): AIT-300-ASTM was used to conduct the impact test. The ASTM International standards (ASTM-E−23) were followed in the preparation of the specimens for the impact tests. The sample before the test is shown in Fig. 3(a). The sample has the following measurements: 55 mm × 10 mm x 10 mm, with a central 2 mm notch. Following surface grinding, diamond paste was used to polish the sample, which was then thoroughly rinsed. It was then cleaned with acetone after being etched for 20 s with Kellar's solution. The sample had finally been prepared to be placed in the Amscope optical microscope to get the microstructures. After that, SEM images were taken and EDS analysis was performed with a JEOL JCM-7000 Neo-Scope SEM running at 10 kV. To get ready for SEM imaging, the samples were coated with gold to avoid the charging effect of the samples. To understand the effect of the Mg addition on the corrosion behavior in aluminum alloy, the samples were immersed into the 3.5 wt % NaCl medium and weight loss and thickness reduction were measured daily.

3. Result and discussion

In Fig. 2(a), the yield strength and tensile strength of pure aluminum are presented, with the yield strength being approximately 32 MPa and the tensile strength being approximately 67 MPa. However, adding Mg led to a significant increase in both yield and tensile strength. This was because the additional Mg strengthened the material through solid solution strengthening and grain boundary refinement, resulting in the formation of the brittle compound Al_3Mg_2 [12–14]. The alloy developed several dislocations when a tensile load was applied. As the load was increased further, the alloy started to distort and the dislocation began to move. The Al_3Mg_2 intermetallic, which formed when magnesium was added to aluminum, was evenly dispersed throughout the alloy. Consequently, the dislocations' movements were restricted because the intermetallic obstructed the dislocation's route of motion. The strength of the aluminum alloys with magnesium added increased as a result of requiring more energy to overcome the intermetallic. This strengthening effect was also observed up to a 5 % Mg addition. The addition of 5 % Mg resulted in a yield strength of approximately 87 MPa and a tensile strength of 108 MPa. However, adding 7 % Mg led to a decrease in both yield and tensile strength. This was due to the coarsening of the Al_3Mg_2 compound, which was less effective at restricting dislocation movement, resulting in a slight decrease in strength [10,11].

Upon examining Fig. 2(b), it becomes apparent that the incorporation of Mg into the aluminum alloy led to a decrease in elongation. Although pure aluminum is ductile, the inclusion of Mg triggered the development of the brittle intermetallic compound Al_3Mg_2 [15]. This compound was responsible for the reduction in elongation that was observed when Mg was introduced to the aluminum alloy by restricting the movements of the dislocations and making it brittle. However, 7 wt % Mg addition has shown more %elongation compared to the 5 wt % Mg added alloy as the intermetallic became coarse which was unable to restrict the movements of the dislocations more efficiently.

The fracture surfaces of the alloys are presented in Fig. 3. For the pure aluminum cup shape fracture surface is found [16]. For the 3 wt % mg added, the alloy also formed almost a cup-shaped fracture surface. However, 5 wt % and 7 wt % addition of Mg induced brittle fracture as the fracture surface was found almost flat. That's why the elongation was decreased with the Mg addition [17].

The flexural strength of aluminum alloy matrix composites with varying amounts of Mg addition (3 wt %, 5 wt %, and 7 wt %) was determined through a three-point bending test. The results, depicted in Fig. 4, reveal that the inclusion of Mg strengthens the material's flexural strength by creating the brittle compound Al_3Mg_2, leading to a noticeable increase in flexural strength compared to pure aluminum. The addition of the Mg alloying element reduced movements of the dislocations at the grain boundaries by developing hindrance by the intermetallic within the matrix [18]. Specifically, the addition of 3 wt % Mg resulted in a 48 % increase in flexural strength, while 5 wt % and 7 wt % Mg led to increases of 64 % and 59 %, respectively. From the graph, the 7 wt % Mg addition decreased the flexural strength by coarsening the intermetallic in the matrix found in the optical and SEM images.

The graph depicted in Fig. 5 shows a strong correlation between the hardness value and the percentage of Mg added to the aluminum alloy. The test results demonstrate that the addition of more Mg led to an increase in the alloy's hardness. Specifically, when 3 wt % Mg was added, and the micro-hardness value of the aluminum alloy rose from 25.4 HB to 34 HB, resulting in a 34.8 % increase. Additionally, increasing the 5 % Mg content resulted in a further 87 % enhancement of the hardness. This is due to the formation of Al_3Mg_2 intermetallic and the refinement of grain, as seen in the optical microscopic images. However, adding 7 % Mg reduced the hardness when compared to adding 5 % Mg. The hardness value for 5 % Mg was 47.56 HB, while for 7 % Mg, it was 43.36 HB, a decline

Fig. 1. a) Prepared tensile test sample and b) Sample after tensile test performed.
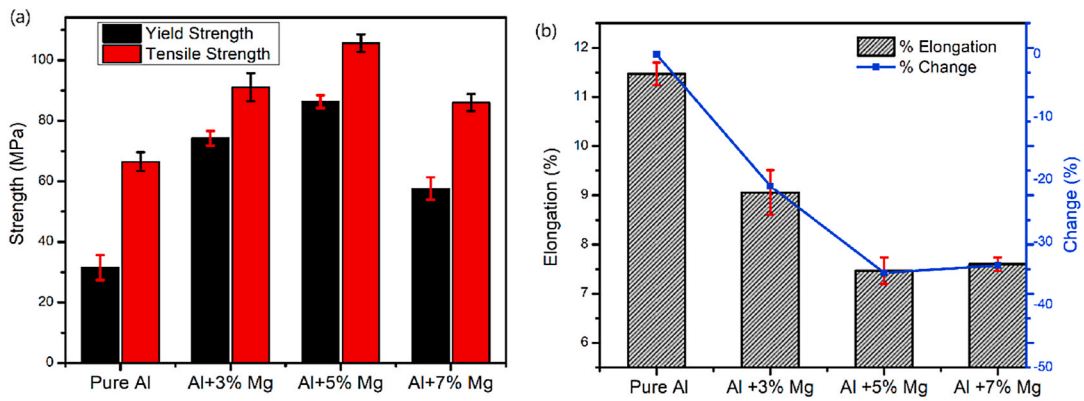
Fig. 2. a) Comparison of yield strength and tensile strength of the Mg-added aluminum alloys b) Percentage of elongation change with the various Mg-added aluminum alloy.
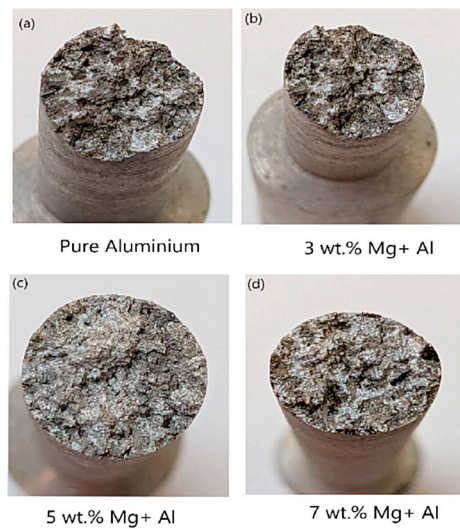
Fig. 3. Demonstration of the fracture surface of the a) pure aluminum b) 3 wt % Mg added aluminum alloy c) 5 wt % Mg added aluminum alloy d) 7 wt % Mg added aluminum alloy after the tensile test.
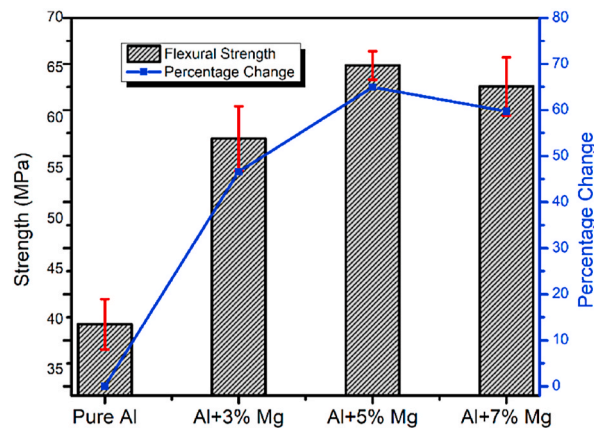
Fig. 4. Flexural strength of the various percentage Mg added aluminum alloy.
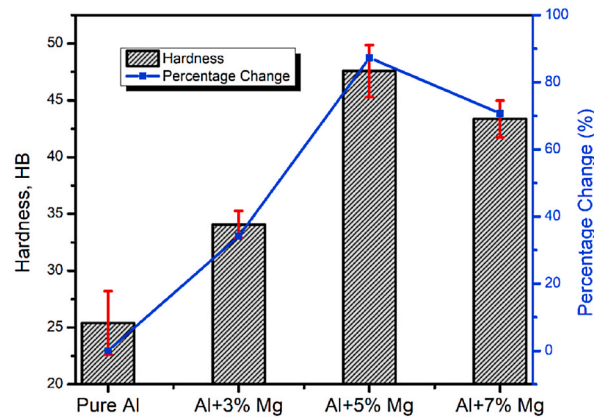
Fig. 5. Variation in hardness with the Mg addition in aluminum alloy.

of almost 9 %. This reduction is likely due to the coarsening of the intermetallic compound Al_3Mg_2 [19].

Fig. 6 depicts a clear relationship between impact energy and the percentage of Mg added to the aluminum alloy. The test results indicate that increasing the magnesium caused the aluminum alloy to become more brittle, which decreased impact energy. The magnesium addition resulted in the formation of an intermetallic that is brittle. An increase in brittleness makes the alloy more prone to failure. As a result, hardly much energy was needed to break down the specimens. Because of this, the alloy with the additional magnesium had a lower impact energy and a lower toughness [15,17]. Specifically, when 3 wt % Mg was added, the impact energy of the aluminum alloy decreased by 11.5 %, from 19.72 J to 17.46 J. Increasing the Mg content to 5 wt % resulted in a further 29.19 % reduction in impact energy, due to the formation of Al_3Mg_2 intermetallic and the resulting drop in toughness, as seen in the optical microscopic images and SEM images. However, adding 7 wt % Mg resulted in a higher impact energy compared to adding 5 wt % Mg. This improvement in toughness is due to the coarsening of the intermetallic compound Al_3Mg_2, which reduces the brittleness effect to a greater extent.

The microstructures of pure aluminum and an aluminum alloy with added Mg are shown in Fig. 7. Pure aluminum displays a visible grain boundary with some impurities (Fig. 7(a)), while the addition of Mg resulted in the formation of Al_3Mg_2, which was visible in the alloy. The addition of 3 % Mg facilitated grain refinement (Fig. 7(b)), leading to increased strength. Additionally, the inclusion of the brittle intermetallic compound reduced dislocation movement, thus contributing to the increase in hardness, tensile strength, and flexural strength [16]. A 5 wt % Mg addition resulted in even better outcomes due to increased intermetallic compound formation and grain refinement (Fig. 7(c)). However, a 7 wt % Mg addition caused the intermetallic compound to become coarseness [14], which decreased the effectiveness of dislocation movement restriction, leading to a slight degradation in strength and hardness values (Fig. 7 (d)). The SEM image of the 5 wt % Mg added aluminum alloy in Fig. 8 shows the clear visibility of the Al_3Mg_2 intermetallic compound.

Fig. 8 displays the SEM images of the fracture surface of pure Al, Al–3 %Mg, Al–5 %Mg, and Al–7 %Mg alloys after the tensile test. The dimples are found for the pure aluminum indicating the ductile fracture behaviors [20–22]. The addition of alloying elements altered the surface morphology of pure aluminum with an intermetallic phase. The addition of Mg resulted in the formation of a eutectic intermetallic phase due to reactions with Al with Mg. At room temperature, the SEM images reveal spherical eutectic Al_3Mg_2 intermetallic phases that are scattered around the Al matrix and grain boundaries (Fig. 8b, c, 8d). These intermetallic particles induced brittleness in the samples as the dimples were not found after the Mg addition. The EDS analysis confirmed the presence of the Al and
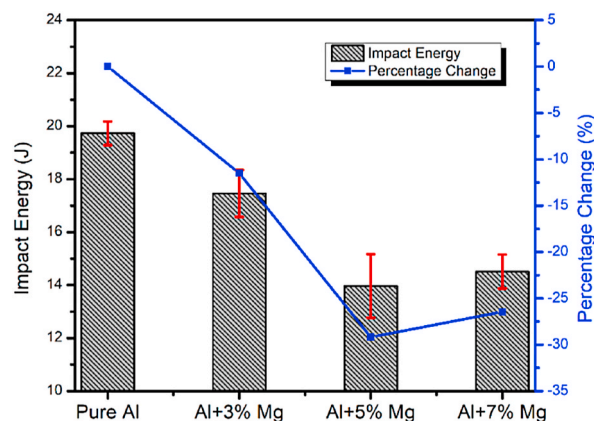
Fig. 6. Variation in impact energy with Mg addition in aluminum alloy.
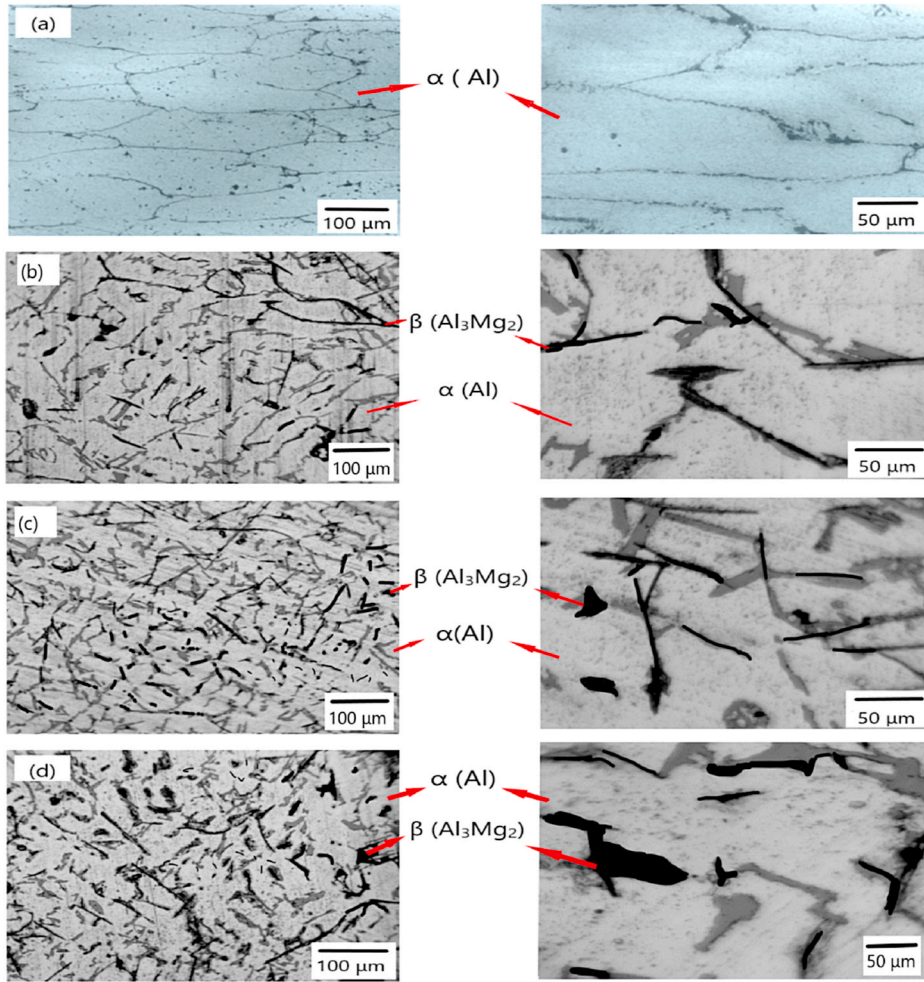
Fig. 7. Optical microscope image of the a) pure aluminum b) 3 wt % Mg added aluminum alloy c) 5 wt % Mg added aluminum alloy d) 7 wt % Mg added aluminum alloy.

Mg within the globular-shaped intermetallic particles indicating the formation of the Al_3Mg_2 intermetallic phases. Line analysis was also conducted of the 5 wt % Mg to ensure the presence of the Al_3Mg_2 intermetallic compound presented in Fig. 9. With the increasing the Mg addition the amounts of the intermetallic formation increased. That's why the addition of 5 wt % Mg increased the strength and hardness along with the reduction of the %elongation and impact energy. The intermetallic Al_3Mg_2 is brittle which is capable of withstanding localized deformation by restricting the movements of the dislocations [23]. However, the 7 wt % Mg addition induced the intermetallic to be coarsened which is visible in the SEM image (Fig. 8(d)). Thus, the restriction of the dislocation motion was not effective like the 5 wt % Mg addition. The strength and hardness values were dropped due to the reduction in brittleness.

The most accurate and precise method of determining metal corrosion rate is through weight-loss measurement. This is because the experimentation involved is easy to replicate and, although it may require long exposure times, it is worth it. In Fig. 10(a), the % weight loss of the alloy is shown as a function of time. Meanwhile, Fig. 10(b) illustrates the variation of instantaneous corrosion rate in terms of the weight loss process with increasing periods of exposure time. To calculate the corrosion rate, process equation (1) is used.

$$\text{Corrosion rate, R} = \frac{534 \times \nabla w}{\rho A t} \tag{1}$$

Where, R = corrosion rate in mm/year; ∇w = (initial weight – final weight) in mg; ρ = density of the sample in mg/m^3; A = area of the sample in m^2; t = time in an hour.

The graph in Fig. 10(c) illustrates the changes in instantaneous corrosion rate, measured in terms of corrosion current density, as the exposure time increases. Gravimetric parameters are converted to electrochemical corrosion rate using Faraday's law shown in equation (2).

$$\text{Corrosion rate, I}_{corr} = \frac{nF\nabla w}{MtA} \tag{2}$$
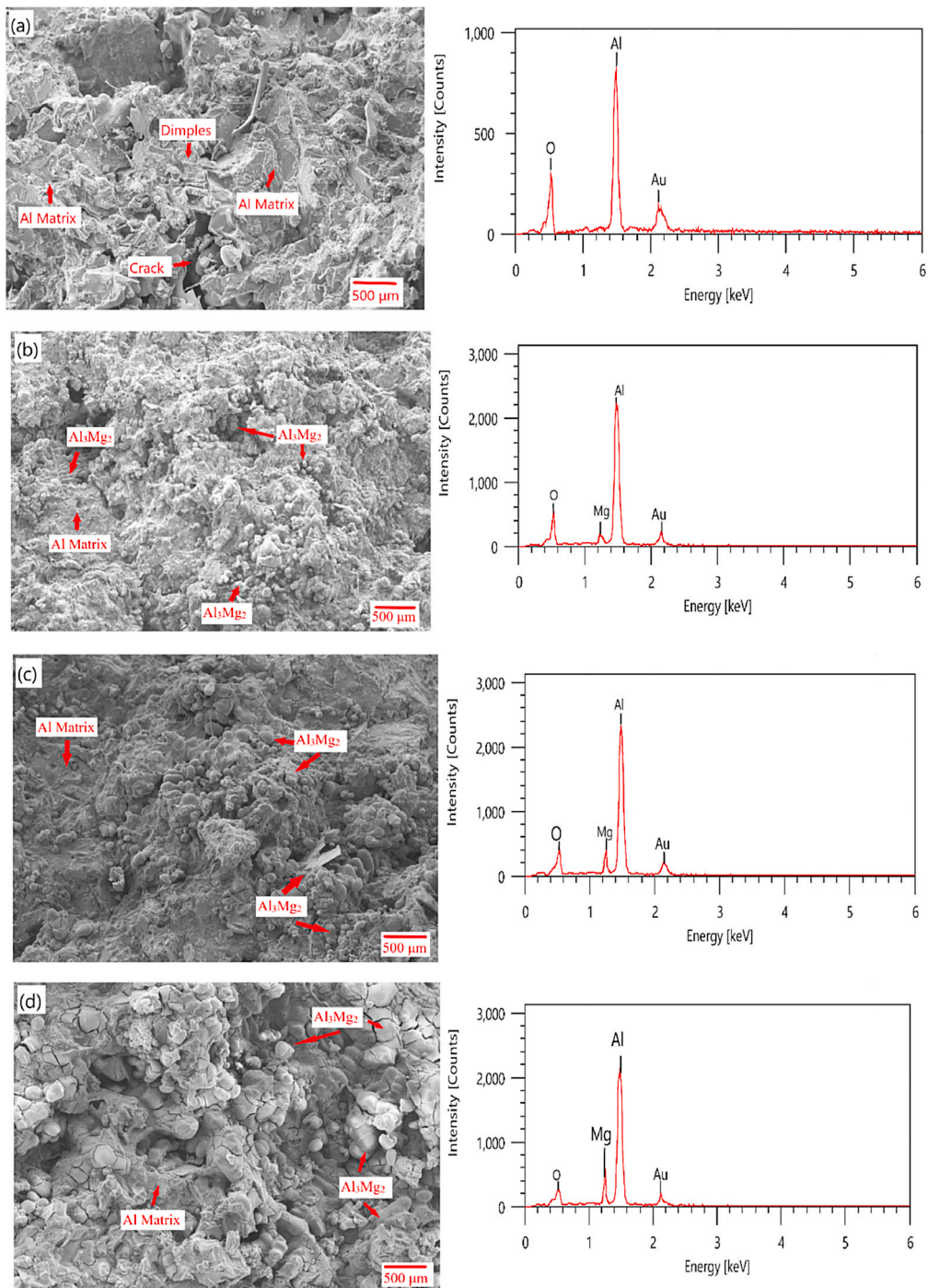
Fig. 8. SEM image of the a) Pure aluminum b) 3 wt % Mg added Al alloy c) 5 wt % Mg added Al alloy d) 7 wt % Mg added Al alloy.

The current density (I_{corr}) in A/cm^2 indicates the corrosion rate, while ∇w represents the weight loss caused by corrosion in grams. The variables n, F, M, t, and A stand for valence, Faraday's constant (96,500 coulombs), the molecular weight of the metal in grams per mole, time in seconds, and the surface area of the metal exposed to corrosion in square centimeters, respectively.

In the experiment, it was observed that pure aluminum had lower weight loss and lower corrosion rate. After 30 days, the weight loss, corrosion rate, and current density were found to be 2.94 %, 5.09×10^{-7} mm/year, and 3.19×10^{-8} A/cm^2 respectively (Fig. 10). However, the weight loss, corrosion rate, and current density became stable after 10 days immersion in 3.5 % NaCl medium. This was due to the formation of the Al$_2$O$_3$ protective layer which made the corrosion rate steady after a short period. However, it was found that
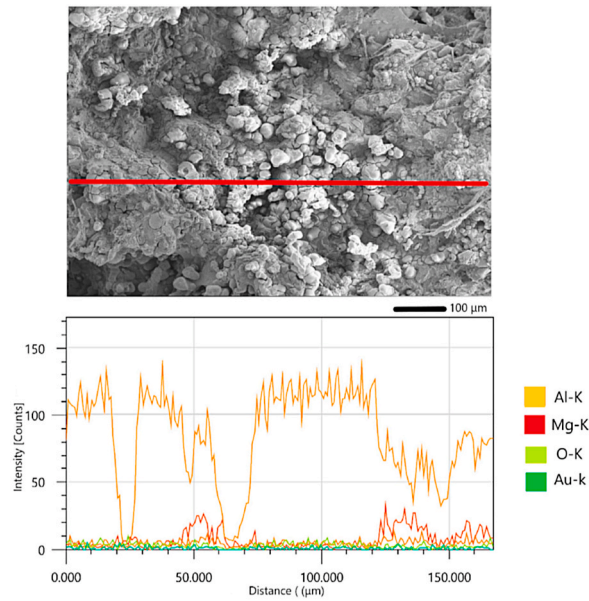
Fig. 9. Line analysis of the 5 % Mg added aluminum alloy.
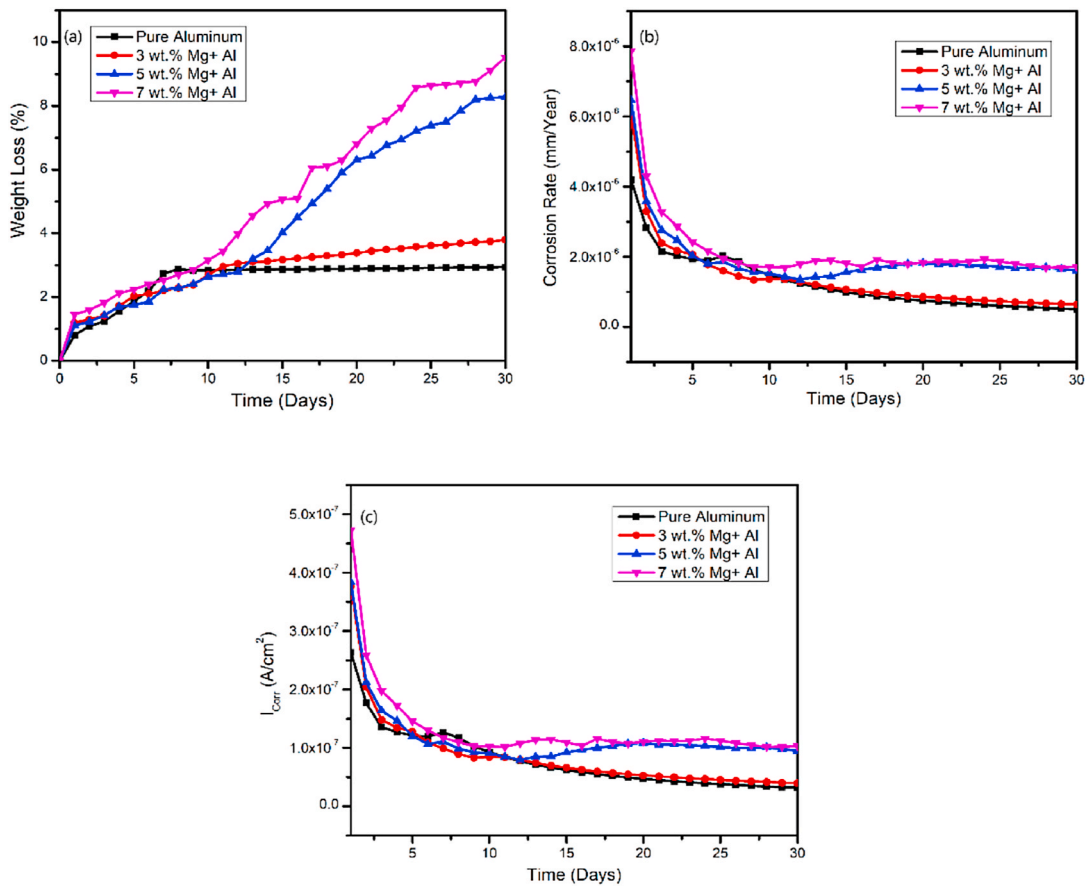
Fig. 10. a) Percentage of weight loss b) Corrosion rate in terms of weight loss c) Corrosion rate in terms of the corrosion current density of the alloy with the exposed time in 3.5 wt % NaCl medium.

the higher the addition of Mg, the higher the weight loss and corrosion rate, as Mg is highly reactive and acts as an anode concerning the Al matrix. Fluctuations in the weight loss and corrosion rate were also observed. When the protective layer was formed for the Mg-added alloy, the corrosion rate was reduced. However, due to the reactive nature of Mg, the protective layer was torn off, resulting in a higher corrosion rate. After 30 days of immersion in NaCl medium, the weight loss for the Al–3 %Mg, Al–5 %Mg, and Al–7 %Mg alloys was found to be 3.8 %, 8.27 %, and 9.52 % respectively (Fig. 10(a)). The corrosion rate for the Al–3 %Mg, Al–5 %Mg added alloys was found stable after 30 days of immersion. However, an increasing trend in both weight loss and corrosion rate was also observed for the Al–7 %Mg alloy due to the presence of a higher concentration of Mg.

The SEM images shown in Figs. 11 and 12 display the corrosion behaviors of the Mg-added aluminum alloy after being immersed in a 3.5 % NaCl medium for fifteen days and thirty days. The surface of the corrosion products formed on the alloy displays concave and convex structures, which indicates localized corrosion [24]. The corrosion products have cracks and pits, which may be due to internal stress or dehydration of hydroxides as Mg-induced stress corrosion cracking. A considerable amount of metal loss from the alloy is observed underneath the original surface, confirming that the alloy is prone to severe localized corrosion after being immersed for five days and seven days in both mediums [25]. In the initial stages of corrosion, a protective surface film of Al_2O_3 was formed above the alloy, leading to high corrosion resistance shown in Fig. 11(a), (b), 11(c) and 11(d). However, severe localized corrosion occurred beneath the surface when the immersion time was passed. As the immersion time increased, the protective layer became distorted due to the presence of Nano-sized pores. The surface potential difference between Al and Al_2Mg_3 phase results in preferential dissolution of Mg near their boundary. The intermetallic phase of Al_2Mg_3 acts as an anode in a micro-galvanic couple and corroded [26]. With longer immersion times, the dissolution of Mg and Al near the exposed secondary phase and the formation of porous corrosion products around it are observed in Figs. 11 and 12. Then, defects on the surface film were generated, and localized corrosion occurred around these defects. Therefore, the degradation of corrosion resistance of the alloy might be attributed to micro galvanic corrosion between Al and Al_2Mg_3 and the resultant breakage of the protective film and produced the crevices and pits within the alloy.

However, thirty days in the corrosion medium resulted in the formation of more pits and crevices, leading to increased weight loss than fifteen days of immersion in the NaCl medium. The protective layer was unable to withstand the corrosion environment for 30 days and failed to protect the Mg-added aluminum alloy as shown in Fig. 12(a), (b), 12(c), and 12(d). As chloride ions presented in the corrosive medium, it caused a rapid dissolution within the pit, while oxygen reduction occurs on adjacent surfaces [27]. An excess of positive charge is produced within the pit, which results in the migration of chloride ions to maintain electro-neutrality. As chloride
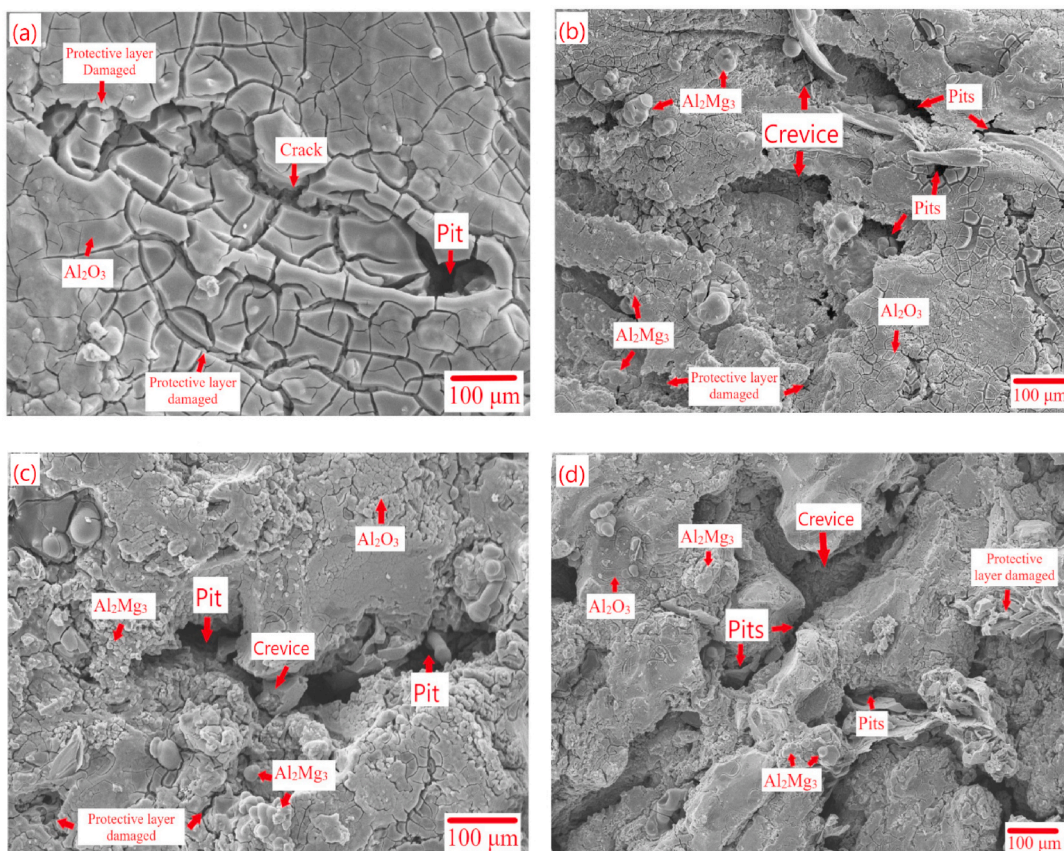
Fig. 11. SEM image of the corroded alloy immersed in 3.5 wt % NaCl medium for 15 days. a) Pure aluminum b) 3 wt % Mg added Al alloy c) 5 wt % Mg added Al alloy d) 7 wt % Mg added Al alloy.
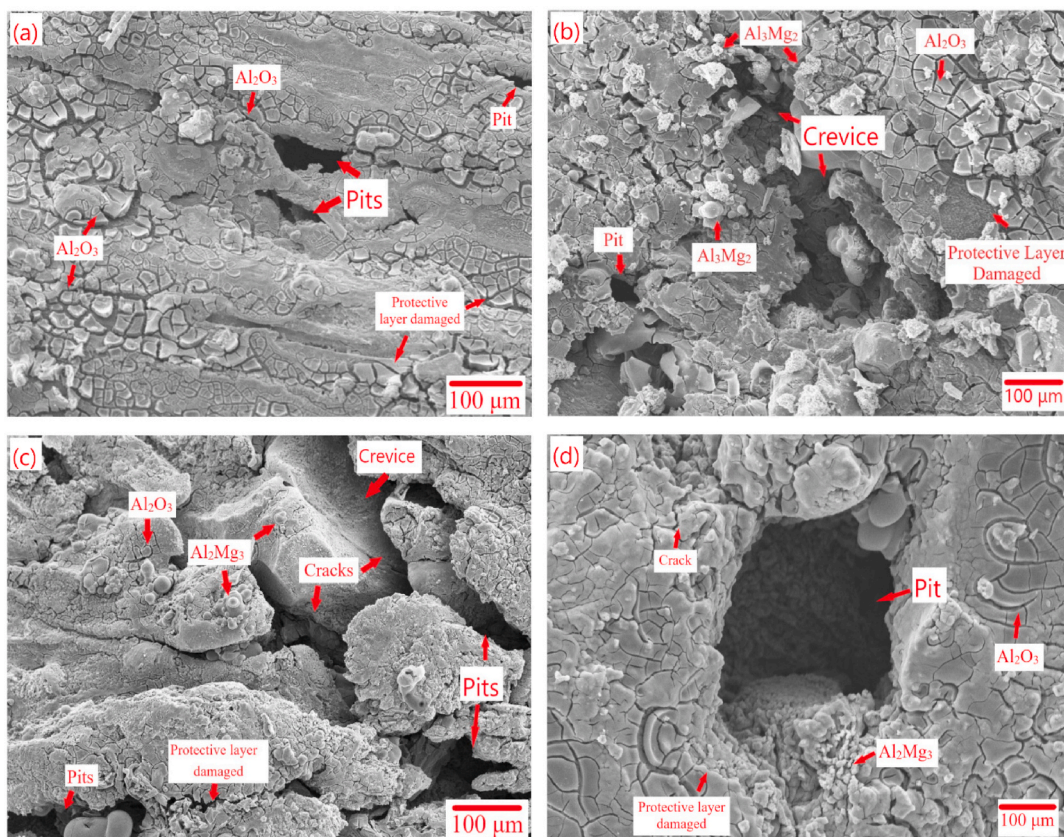
Fig. 12. SEM image of the corroded alloy immersed in 3.5 wt % NaCl medium for 30 days. a) Pure aluminum b) 3 wt % Mg added Al alloy c) 5 wt % Mg added Al alloy d) 7 wt % Mg added Al alloy.

ions migrated from the NaCl medium, it caused a high concentration of chloride ions within the pit. This high concentration of chloride ions stimulates the dissolution of most metals and alloys, ultimately accelerating the entire process over time. Since the solubility of oxygen is virtually zero in concentrated solutions, no oxygen reduction occurs within a pit [28,29].

An analysis of maps was conducted on 3.5 wt % NaCl corroded samples to gain a better understanding of their corrosion behavior shown in Fig. 13. In the pure aluminum sample, a protective layer of Al_2O_3 had formed, which resulted in the presence of a lot of oxygen in the map analysis (Fig. 13(a)). Similarly, in the Mg-added aluminum alloy, oxygen was also present due to the protective layer, but the presence of Mg was found to be very small as shown in Fig. 13(b), (c) and 13(d). The intermetallic Al_2Mg_3 acted as an anode, and as a result, the amount of Mg present was reduced due to its dissolution into the NaCl solution [30]. In the case of the 7 wt % Mg added alloy, the dissolution was higher as the map showed lower amounts of Mg presence. This resulted in the observation of more and larger pits for the 7 wt % Mg added aluminum alloy in the NaCl solution.

To better understand the corrosion behavior of the aluminum alloy schematic diagram is presented in Fig. 14. Initially, when the alloy comes in contact with aqueous solutions, it forms a protective film on its surface. This film reduces the corrosion rate by preventing the alloy from coming into direct contact with the corrosive species [30–32]. The presence of Al in the matrix enhances the corrosion resistance by reacting with oxygen to form a corrosion product film Al_2O_3. However, the surface film has tiny pores at the metal/film interface. As the immersion time increases, the pores inside the film allow corrosive species such as chloride ions to diffuse through the film [33,34]. This causes the corrosion of magnesium present in the intermetallic and breakage of the surface film, as shown in the figure. The highly reactive nature of magnesium also induces stress-cracking corrosion, which damages the protective films. Consequently, the protective effect of the surface film is undermined, and severe localized corrosion occurs around these defects, leading to the dissolution of the metal and forming pits [35]. Therefore, the stability of the surface film is critical to the high corrosion resistance of the aluminum alloy. Furthermore, when chloride ions migrate from acidic and NaCl media, they cause a high concentration of chloride ions within the pit, which stimulates the dissolution of most metals and alloys, ultimately accelerating the entire process over time. The SEM images of the corroded samples reveal the damaged Al_2O_3 protective layer and the formation of numerous pits and cracks due to the dissolution of the alloy. The map analysis of the samples also reveals the corrosion behaviors due to the presence of higher oxygen over the surface of the corroded samples (Fig. 13).

As the addition of Mg in aluminum led to the breakdown of the Al_2O_3 protective layer and corroded the alloy, less amount of Mg addition is preferable. For this reason 5 wt % Mg added alloy is the best choice considering the improvement in mechanical properties
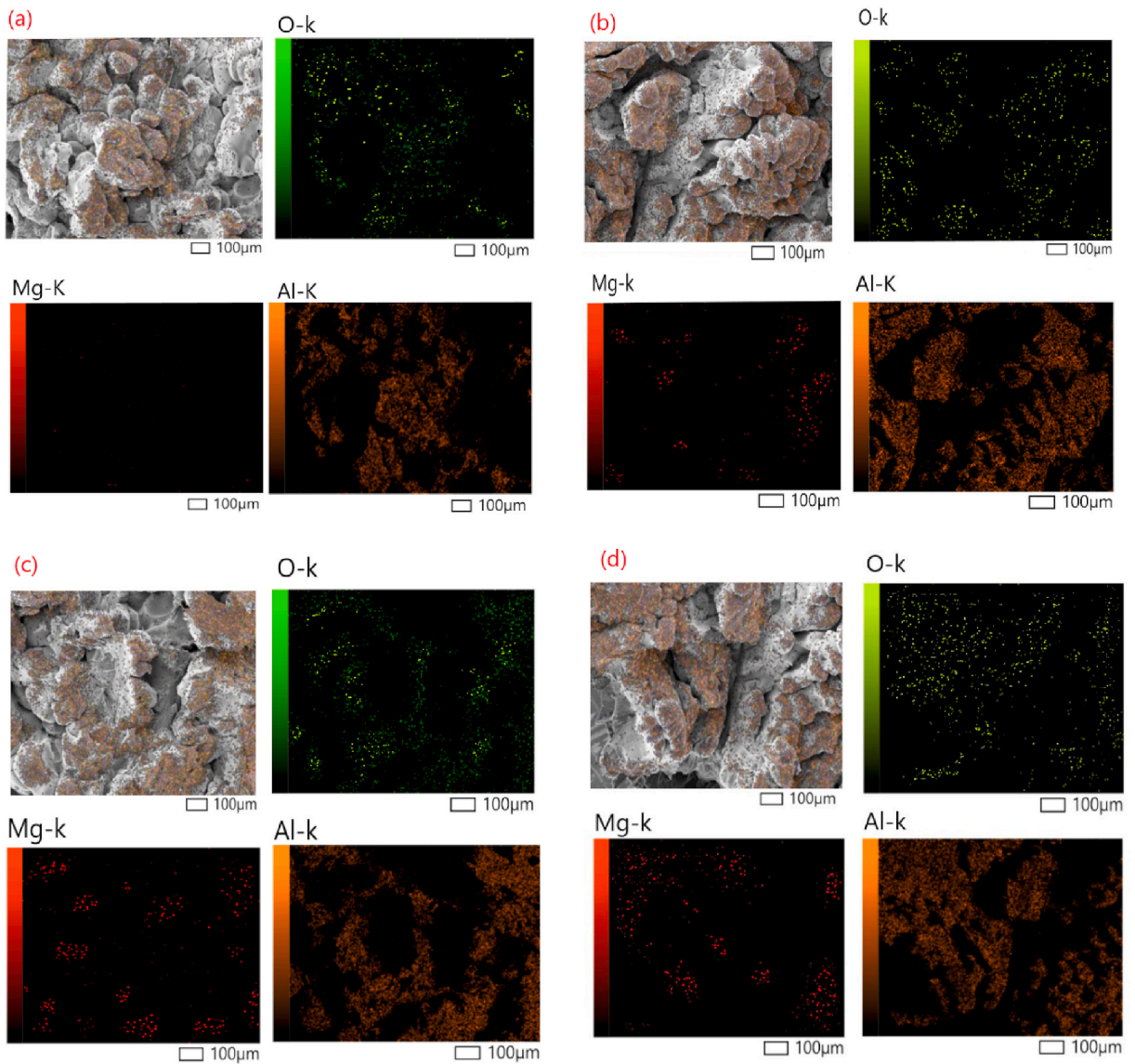
Fig. 13. SEM image of the corroded alloy immersed in 3.5 wt % NaCl medium for 10 days. a) Pure aluminum b) 3 wt % Mg added Al alloy c) 5 wt % Mg added Al alloy d) 7 wt % Mg added Al alloy.
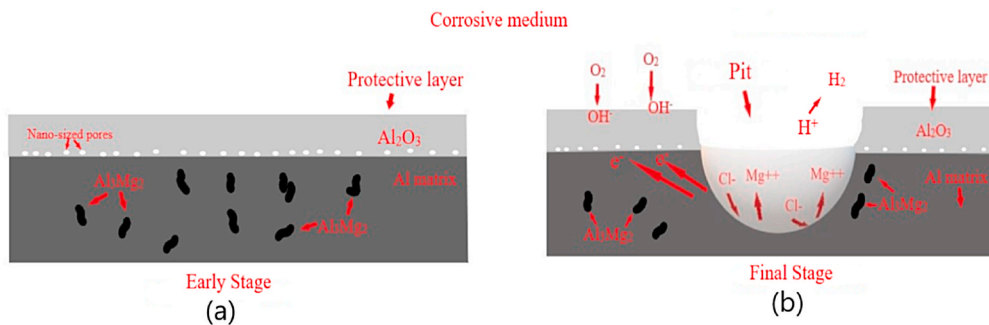
Fig. 14. Schematic diagram of corrosion behavior and pit formation of Mg-added aluminum alloy. (a) The initial stage of pit formation and (b) The final stage of pit formation of the Mg-added aluminum alloy.

and lower corrosion rate. However, introducing the Cr and Fe in the Mg-added aluminum alloy may improve the protective layer and reduce the corrosion rate.

4. Conclusion

The experiment was conducted to study the effects of adding Mg to an aluminum alloy with varying concentrations of 3 wt %, 5 wt %, and 7 wt %. The inclusion of 5 wt % Mg led to the formation of brittle intermetallic Al_3Mg_2, which enhanced the alloy's strength and hardness by about 59 % and 87 % respectively by limiting dislocation movement and promoting grain refinement. After the addition of 5 wt % Mg, the impact energy, and % elongation of aluminum alloys decreased by 29.19 % and 34.87 % respectively, leading to reduced toughness and ductility. The optical microstructure and SEM images revealed refined grains and the formation of Al_3Mg_2, providing valuable insight into Mg's strengthening behavior in aluminum. However, 7 wt % Mg addition has shown a negative impact in improving the strength compared to the 5 wt % Mg added alloy as the intermetallic became coarse which was unable to restrict the movements of the dislocations more efficiently. The grain coarsening of the 7 wt % Mg added alloy was also revealed in the optical and SEM microscope images. The EDS analysis confirmed the presence of the Al and Mg within the globular-shaped intermetallic particles indicating the formation of the Al_3Mg_2 intermetallic phases. It has been observed that the alloy experiences a significant amount of metal loss beneath the original surface when immersed in 3.5 wt % NaCl medium for a period of fifteen and thirty days. However, the weight loss, corrosion rate, and current density became stable for pure aluminum after 10 days of immersion in a 3.5 % NaCl medium due to the Al_2O_3 protective layer. The highly reactive nature of magnesium contributes to stress-cracking corrosion, which damages the protective films and leads to metal dissolution, causing the formation of pits and cracks. The weight loss for the Al–3 %Mg, Al–5 % Mg, and Al–7 %Mg alloys after 30 days of immersion in NaCl medium was determined to be 3.8 %, 8.27 %, and 9.52 %, respectively. After 30 days of immersion, the corrosion rates for the alloys with Al-3 % and Al-5 % added were found to be steady. On the other hand, because of the higher Mg concentration, a rising trend in weight loss and corrosion rate has been observed for the Al–7 %Mg alloy. Upon conducting SEM analysis of the corroded samples, it was observed that the aluminum alloy exhibited pit formation as a result of the breakdown of the Al_2O_3 protective layer after being immersed in 3.5 wt % NaCl. Al–5 %Mg is found to be the optimum level for the addition of Mg in aluminum to improve strength and hardness without sacrificing the alloy's toughness and ductility. This is due to the alloy's lower corrosion rate and refined Al_3Mg_2 intermetallic compound.

Data availability statement

No data was used for the research described in the article.

Additional information

No additional information is available for this paper.

CRediT authorship contribution statement

Mohammad Salman Haque: Conceptualization, Methodology, Writing – original draft, Software, Data curation, Visualization, Writing – original draft, Investigation. **Modassher Nomani:** Conceptualization, Methodology, Writing – review & editing, Software. **Azmery Akter:** Conceptualization, Supervision, Resources. **Istiak Ahmed Ovi:** Methodology, Visualization, Software.

Declaration of competing interest

The authors declare that they have no known competing financial interests or personal relationships that could have appeared to influence the work reported in this paper.

Acknowledgement

References

[1] M. Hussain, S. Nawaz, M. Sajid, A. Nawaz, A. Irum, Y. Javed, C. Ge, G. Yasin, Corrosion resistance of nanostructured metals and alloys, Corros. Protect. Nanoscale (2020) 63–87.

[2] n. rokon, m. s. haque, m. s. kaiser, On the mechanical behaviour of thermally affected non-heat-treatable aluminium alloys, journal of chemical technology & metallurgy 58 (6) (2023).

[3] K. Chen, L. Zhan, W. Yu, Rapidly modifying microstructure and mechanical properties of AA7150 AL alloy processed with electroplating treatment, J. Mater. Sci. Technol. 95 (2021) 172–179, https://doi.org/10.1016/j.jmst.2021.03.060.

[4] Mohammadi, et al., Developing age-hardenable al-Zr alloy by ultra-severe plastic deformation: Significance of supersaturation, segregation and precipitation on hardening and electrical conductivity, Acta Mater. 203 (2021) 116503, https://doi.org/10.1016/j.actamat.2020.116503.

[5] M. Kaiser, Effect of trace impurities on the thermoelectric properties of commercially pure aluminum, Mater. Phys. Mech. 47 (2021) 582–591, https://doi.org/10.18149/MPM.4742021_5.

[6] M. Haque, S. Khan, M. Kaiser, Effect of Sc and Zr on precipitation behaviour of wrought Al- bronze, IOP Conf. Series: Mater. Sci. Eng. 1248 (1) (2022).

[7] J. Lazaro-Nebreda, et al., De-ironing of aluminum alloy melts by high shear melt conditioning technology: an overview, Metals 12 (10) (2022) 1579, https://doi.org/10.3390/met12101579.

[8] K.N. Uday, G. Rajamurugan, Influence of process parameters and its effects on friction stir welding of dissimilar aluminum alloy and its composites – a Review, J. Adhesion Sci. Technol. (2022) 1–34, https://doi.org/10.1080/01694243.2022.2053348.

[9] F. Czerwinski, Critical assessment 40: a search for the eutectic system of high-temperature cast aluminum alloys, Mater. Sci. Technol. 37 (7) (2021) 683–692, https://doi.org/10.1080/02670836.2021.1940670.

[10] T. Trzepiecinʹ ski, et al., Recent developments and future challenges in incremental sheet forming of aluminum and aluminum alloy sheets, Metals 12 (1) (2022) 124, https://doi.org/10.3390/met12010124.

[11] M.S. Haque, S.N. Rokon, M.S. Kaiser, Strengthening and softening behavior of non-heat-treatable aluminum alloys subject to deformation and annealing treatment, Mater. Today: Proc. 82 (2023) 151–157.

[12] Q. Zheng, et al., Effect of micro-alloying element La on corrosion behavior of AlMg-Si Alloys, Corros. Sci. 179 (2021), https://doi.org/10.1016/j.corsci.2020.109113.

[13] V.V. Zakharov, Aluminum alloys for additive technologies, Metal Sci. Heat Treatm. 63 (5–6) (2021) 231–235, https://doi.org/10.1007/s11041-021-00676-8.

[14] W. Xu, et al., Stress corrosion cracking resistant nanostructured al-mg alloy with low angle grain boundaries, Acta Mater. 225 (2022) 117607, https://doi.org/10.1016/j.actamat.2021.117607.

[15] K. Hirayama, H. Toda, D. Fu, R. Masunaga, H. Su, K. Shimizu, A. Takeuchi, M. Uesugi, Damage micromechanisms of stress corrosion cracking in Al-Mg alloy with high magnesium content, Corros. Sci. 184 (2021).

[16] Øyvind Ryen, Bjørn Holmedal, Oscar Nijs, Erik Nes, Emma Sjölander, Hans-Erik Ekström, Strengthening mechanisms in solid solution aluminum alloys, Metall. Mater. Trans. 37 (2006) 1999–2006.

[17] Wenwen Sun, Yuman Zhu, Ross Marceau, Lingyu Wang, Qi Zhang, Xiang Gao, Christopher Hutchinson, "Precipitation strengthening of aluminum alloys by room-temperature cyclic plasticity.", Science 363 (6430) (2019) 972–975.

[18] Kaka Ma, Haiming Wen, Tao Hu, Troy D. Topping, Dieter Isheim, David N. Seidman, Enrique J. Lavernia, Julie M. Schoenung, Mechanical behavior and strengthening mechanisms in ultrafine grain precipitation-strengthened aluminum alloy, Acta Mater. 62 (2014) 141–155.

[19] Lavish K. Singh, Alok Bhadauria, Laha Tapas, Comparing the strengthening efficiency of multiwalled carbon nanotubes and graphene nanoplatelets in aluminum matrix, Powder Technol. 356 (2019) 1059–1076.

[20] Xiaoguang Yu, Guohua Xing, Zhaoqun Chang, Flexural behavior of reinforced concrete beams strengthened with near-surface mounted 7075 aluminum alloy bars, J. Build. Eng. 31 (2020) 101393.

[21] Xiaoxu Huang, N. Kamikawa, N. Hansen, Strengthening mechanisms in nanostructured aluminum, Mater. Sci. Eng. 483 (2008) 102–104.

[22] Shraboni Sarker, Mohammad Salman Haque, Md Sadbin Azad Alvy, Md Mehedi Hasan Abir, The effects of solution heat treatment on the microstructure and hardness of an aluminum-4% copper alloy with added nickel and tin, Journal of Alloys and Metallurgical Systems 4 (2023) 100042.

[23] Srinivasa R. Bakshi, Arvind Agarwal, "An analysis of the factors affecting strengthening in carbon nanotube reinforced aluminum composites.", Carbon 49 (2) (2011) 533–544.

[24] Yuyao Li, Shun Meng, Qianming Gong, Yilun Huang, Jianning Gan, Ming Zhao, Bin Liu, Lei Liu, Guisheng Zou, Daming Zhuang, Experimental and theoretical investigation of laser pretreatment on strengthening the heterojunction between carbon fiber-reinforced plastic and aluminum alloy, ACS applied materials & interfaces 11 (24) (2019) 22005–22014.

[25] Jian Lan, Xuejun Shen, Juan Liu, Hua Lin, Strengthening mechanisms of 2A14 aluminum alloy with cold deformation prior to artificial aging, Mater. Sci. Eng. 745 (2019) 517–535.

[26] Zai-meng Qiu, Rong-chang Zeng, Fen Zhang, S.O.N.G. Liang, Shuo-qi Li, Corrosion resistance of Mg− Al LDH/Mg (OH) 2/silane− Ce hybrid coating on magnesium alloy AZ31, Trans. Nonferrous Metals Soc. China 30 (11) (2020) 2967–2979.

[27] Pan Deng, Wenfeng Mo, Zuoqiong Ouyang, Junwei Chen, Binghui Luo, Zhenhai Bai, Effect of Zr content on corrosion behavior and chemically-milled surface roughness of Al-Cu-Mg alloy, J. Alloys Compd. 965 (2023) 171364.

[28] Peng-Peng Wu, Guang-Ling Song, Yi-Xing Zhu, Zhen-Liang Feng, Da-Jiang Zheng, The corrosion of Al-supersaturated Mg matrix and the galvanic effect of secondary phase nanoparticles, Corrosion Sci. 184 (2021) 109410.

[29] Fenjun Liu, Ji Yan, Zhiyong Sun, Jianbo Liu, Yanxia Bai, Zhikang Shen, Enhancing corrosion resistance and mechanical properties of AZ31 magnesium alloy by friction stir processing with the same speed ratio, J. Alloys Compd. 829 (2020) 154452.

[30] Guangyu Li, Wenming Jiang, Feng Guan, Junwen Zhu, Zheng Zhang, Zitian Fan, Microstructure, mechanical properties and corrosion resistance of A356 aluminum/AZ91D magnesium bimetal prepared by a compound casting combined with a novel Ni-Cu composite interlayer, J. Mater. Process. Technol. 288 (2021) 116874.

[31] W. Xu, Y.C. Xin, B. Zhang, X.Y. Li, Stress corrosion cracking resistant nanostructured Al-Mg alloy with low angle grain boundaries, Acta Mater. 225 (2022) 117607.

[32] Dongdong Gu, Han Zhang, Donghua Dai, Chenglong Ma, Hongmei Zhang, Yuxin Li, Shuhui Li, Anisotropic corrosion behavior of Sc and Zr modified Al-Mg alloy produced by selective laser melting, Corrosion Sci. 170 (2020) 108657.

[33] Jiyuan Zhu, Haojie Jia, Kaijin Liao, Xianxuan Li, Improvement on corrosion resistance of micro-arc oxidized AZ91D magnesium alloy by a pore-sealing coating, J. Alloys Compd. 889 (2021) 161460.

[34] Yao Yang, Sijun Cao, Ying Tao, Fuyong Cao, Jingya Wang, Qingchun Zhu, Xiaoqin Zeng, The effects of a corrosion product film on the corrosion behavior of Mg-Al alloy with micro-alloying of yttrium in a chloride solution, Corrosion Communications 11 (2023) 12–22.

[35] Huilong Zhong, Shengci Li, Jiali Wu, Hongling Deng, Jiqiang Chen, Na Yan, Zixin Chen, Liangbo Duan, Effects of retrogression and re-aging treatment on precipitation behavior, mechanical and corrosion properties of a Zr+ Er modified Al-Zn-Mg-Cu alloy, Mater. Char. 183 (2022) 111617.